IOP Conf. Series: Materials Science and Engineering **301** (2018) 012056 doi:10.1088/1757-899X/301/1/012056

Confinement of NORMAL- AND HIGH-STRENGTH CONCRETE by Shape Memory Alloy (SMA) Spirals

A Gholampour[1] and T Ozbakkaloglu[2*]

[1] School of Civil, Environmental and Mining Engineering, University of Adelaide, South Australia 5005, Australia
[2] School of Civil, Environmental and Mining Engineering, University of Adelaide, South Australia 5005, Australia.
Email: togay.ozbakkaloglu@adelaide.edu.au

Abstract. This paper presents the results of an experimental study on the axial compressive behaviour of normal- and high-strength concrete (NSC and HSC) confined by shape memory alloy (SMA) spirals. A spiral pitch space of 36 and 20 mm was used for SMA confinement of NSC and HSC columns, respectively. The confining pressure was applied on the concrete cylinders by SMA spirals that were prestrained at 0, 5.5, and 9.5%. The compression test results on the SMA-confined specimens indicate that the prestrain level of SMA significantly affects the axial compressive behaviour of both NSC and HSC. An increase in the level of prestrain leads to an increase in the peak axial stress and corresponding strain of SMA-confined concrete.

1. Introduction

It is now well understood that lateral confinement of concrete enhances its strength and ductility [1-13]. In most general terms the lateral confinement can be classified under two categories, namely as active and passive confinement. In passive confinement, the confining pressure develops under lateral dilation of concrete subjected to axial compression, whereas in active confinement, a constant confining pressure is present independent of the lateral expansion of the concrete [14-22]. It was shown that active confinement is more effective in enhancing the compressive strength of concrete compared to the passive confinement [14, 15, 17].

Most of the existing studies in the literature on the behavior of actively confined concrete used mechanically prestressed materials or triaxial testing devices to provide confining pressure on the concrete [15, 23-26]. However, because of practical limitations in prestressing the concrete, the application of active confinement in practice has so far been limited [23]. In recent years, a new class of smart material known as shape memory alloy (SMA) has been used to actively confine the concrete specimens. SMA, a class of metallic alloys, is known for its ability in recovering the original shape after experiencing a large strain (i.e. up to 8%) because of its shape memory effect (at martensitic phase) and superelastic behavior (at austenitic phase) [27].

In recent years, a number of studies have been conducted to understand the mechanical performance of concrete confined by SMAs [28-31]. The results of existing studies revealed that improved mechanical behavior makes SMA a promising material for concrete confinement in the preparation of high performance composite. However, the existing studies only investigated the behavior of SMA-confined normal-strength concrete (NSC). Therefore, additional studies are required to understand the behavior of SMA-confined HSC.

The study presented in this paper was aimed at investigating the compressive behavior of NSC and HSC columns confined by SMA spirals. The results of this study, especially for HSC, help to establish

the possibility of the use of SMA spirals as a confinement technique to produce high performance composite structural members in the construction industry.

2. Test Program

2.1. Test Specimens and Materials

Circular NSC and HSC specimens with a diameter of 100 mm and height of 200 mm were prepared using two grades of concretes with 28-day target unconfined compressive strengths (f'_{co}) of 25 and 65 MPa. Crushed basalt stone with a nominal maximum size of 10 mm were used as the coarse aggregate. The HSC mix contained a polycarboxylic ether polymer-based superplasticizer. NSC and HSC mixes had a water-to-cement ratio (*w/c*) of 0.74 and 0.44, respectively. 16 concrete cylinder were prepared in eight groups, including two control groups (unconfined NSC and HSC), two NSC and HSC groups with unstrained SMA confinement, two NSC and HSC groups with 5.5% prestrained SMA confinement, and two NSC and HSC groups with 9.5% prestrained SMA confinement. The prestraining levels were selected based on the recovery stress (the stress recovered when the deformed wire is heated beyond its transition temperature) applied by SMA by keeping the recovery stress at 35% and 70% of the austenitic rupture stress (referred to as the tensile strength in this paper). Two nominally identical specimens were tested for each confinement configuration.

A nickel (Ni)-titanium (Ti) SMA spiral with diameter of 3.5 mm, manufacturer-specified tensile strength of 1021 MPa, and transition temperature of 77 ℃ was used in this study to confine concrete columns. Figure 1 shows the tensile stress-strain relationship of the SMA wire at martensitic (shape memory behaviour) and austenitic (superelastic behaviour) phases as obtained from tension tests on SMA wires. As can be seen in the figure, a plateau was created in the stress-strain curve of SMA wire at the martensitic phase between 0.01 and 0.04 strain, which is followed by a steep hardening behaviour. The wire finally ruptured at 880 MPa tensile strength and corresponding axial strain of 0.34. It can also be seen in Fig. 1 that, in the austenitic phase, SMA wire failed at a tensile strength of 790 MPa and corresponding strain of 0.21, indicating that SMA developed a 10.2% and 38.2% lower tensile strength and strain, respectively, at austenitic phase than at the martensitic phase.

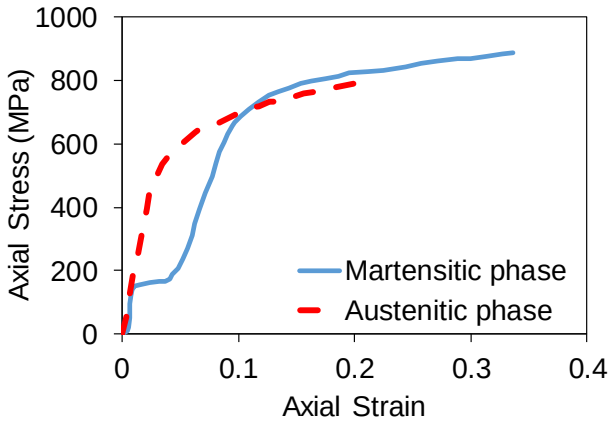

Figure 1. Tensile stress-strain relationship of SMA wire at martensitic and austenitic phases.

Table 1 shows the summary of tension test results on SMA wires. As can be seen in the table, prestrained SMA wires exhibited an average tensile strength of approximately 795 MPa, which is similar to that of unstrained SMA wire at the austenitic phase. This indicates that the tensile strength of SMA is independent to the magnitude of the prestrain induced to the wire.

Table 1. Results of tensile strength tests of SMA wire.

Type of test	Phase	Temperature* (℃)	Level of prestrain (%)	σ_{max} (MPa)	ε_{max} (%)
Uniaxial	Martensitic	17	0	880	34.0
Uniaxial	Austenitic	90	0	795	21.0
Uniaxial	Austenitic	90	5.5	800	15.5
Uniaxial	Austenitic	90	7.5	788	13.5
Uniaxial	Austenitic	90	9.5	794	11.5

* Temperature of SMA wire at the beginning of tension test
σ_{max} = tensile strength; ε_{max} = tensile rupture strain; Temperature

2.2. Instrumentation and Testing Procedures

A single continuous SMA spiral was wrapped around the NSC and HSC specimens with a spiral pitch space of 36 and 20 mm, respectively. The SMA spirals were then heated using a variable AC transformer (with low voltage and high current supply) to the austenitic finish temperature (90 ℃) by passing an electrical current through the wire. After that, the specimens were tested using a 1000-kN capacity universal testing machine under axial compression with displacement control at a rate of 0.18 mm/min. The axial strains of the specimens were measured by two linear variable displacement transformers (LVDTs) mounted at the corners of steel loading and supporting steel plates. Two axial strain gauges mounted at the mid-height of the specimen were also used to validate and correct the LVDT measurements at the early stages of the loading. Figure 2 shows the instrumentation and test setup used in the compression tests.

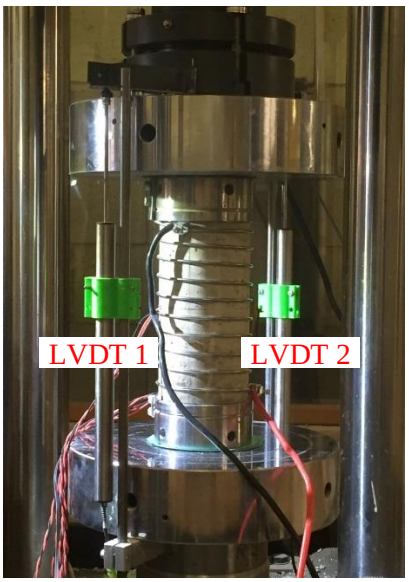

Figure 2. Instrumentation and test setup used in compression tests.

3. Test Results

3.1. Failure Modes

Figure 3 shows typical failure modes of NSC and HSC specimens under SMA confinement. As can be seen in Fig. 3(a), NSC specimens failed by the formation and progression of heterogenic micro-cracks and surface spalling of concrete. On the other hand, HSC specimens failed as a result of the formation

of a major diagonal macro-crack (Fig. 3(b)), which progressed to a sudden rupture of the SMA wire after excessive lateral expansion of concrete.

(a) (b)

Figure 3. Typical failure modes of SMA-confined (a) NSC and (b) HSC.

3.2. Axial stress-Strain Relationship

Table 2 shows the results of the compression test of SMA-confined concrete specimens. The results were averaged from two nominally identical specimens. In the table, the number after NSC and HSC represents the prestraining level. The initial (f_{li}) and ultimate confining pressure (f_{lu}) were calculated using the recovery stress (279 MPa for 5.5% and 558 MPa for 9.5% prestrain level) and tensile strength (795 MPa) of SMA wire, respectively. Based on the axial compression tests on unconfined specimens, f'_{co} of NSC and HSC were obtained as 24.9 and 63.5 MPa and their corresponding axial strain (ε_{co}) were obtained as 0.24 and 0.28%, respectively.

Table 2. Results of uniaxial compression tests on SMA-confined concrete specimens.

Specimen	f'_{co} (MPa)	Level of prestrain (%)	s (mm)	f_{li} (MPa)	f_{lu} (MPa)	f^*_{cc} (MPa)	ε^*_{cc} (%)
NSC-0	24.9	0	36	0	4.25	29.3	0.67
HSC-0	63.5	0	20	0	7.65	67.8	0.68
NSC-5.5	24.9	5.5	36	1.49	4.25	31.0	0.88
HSC-5.5	63.5	5.5	20	2.68	7.65	69.4	0.74
NSC-9.5	24.9	9.5	36	2.98	4.25	34.4	1.04
HSC-9.5	63.5	9.5	20	5.37	7.65	78.5	1.25

f'_{co} = unconfined compressive strength; s = pitch spacing of SMA spiral; f_{li} = initial confining pressure; f_{lu} = ultimate confining pressure; f^*_{cc} = peak axial stress; ε^*_{cc} = axial strain corresponding to f^*_{cc}

As can be seen in Table 2, an increase in the prestrain level resulted in an increase in the peak axial stress (f^*_{cc}) and corresponding strain (ε^*_{cc}) of the specimens. The results show that confinement of NSC specimens with 0%, 5.5%, and 9.5% prestrained SMA spirals resulted in 17.7%, 24.5%, and 38.1% increase in f^*_{cc} and 179.2%, 266.7%, and 333.3% increase in ε^*_{cc}, respectively, compared to those of unconfined NSC specimens. As can be seen in Table 2, confinement of HSC specimens with 0%, 5.5%, and 9.5% prestrained SMA spirals led to 6.8%, 9.3%, and 23.6% increase in f^*_{cc} and 142.9%, 164.3%, and 346.4% increase in ε^*_{cc}, respectively, than those of unconfined HSC specimens. The enhancement in f^*_{cc} and ε^*_{cc} with an increase in the prestrain level of SMA spirals is attributed to the

presence and magnitude of the active confining pressure on specimens confined by prestrained SMA spirals.

Figures 4(a) and (b) show the axial stress-axial strain curves of one of the NSC and HSC specimens under different levels of SMA prestrain, respectively. Comparison of Figs. 4(a) and (b) indicates that SMA confinement of NSC specimens led to a more shallow descending branch in the post-peak curve of the axial stress-strain relationship compared to that of HSC specimens even under a lower level of lateral confinement (as defined by f_{li} and f_{lu}). It can also be seen in the figure that the failure of SMA-confined HSC specimens took place at a lower axial strain compared to that of SMA-confined NSC specimens. These can be attributed to the more brittle behaviour of HSC as was noted in Section 3.1 and discussed in detail in previous studies [32-38].

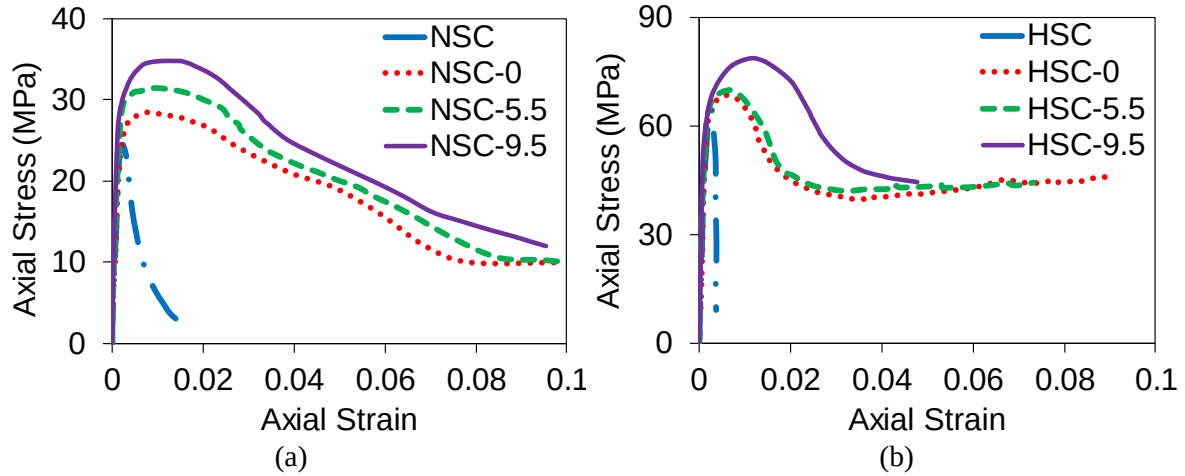

Figure 4. Axial stress-strain curves of SMA-confined (a) NSC; (b) HSC.

4. Conclusions

This paper has presented the results of an experimental study on the axial compressive behaviour of NSC and HSC under SMA confinement. The results showed that SMA confinement significantly increases the compressive strength and corresponding axial strain of NSC and HSC specimens. An increase in the prestrain level results in an increase in the peak axial stress and corresponding axial strain of SMA-confined concrete. Owing to the more brittle behaviour of HSC, SMA-confined HSC fails at a lower axial strain compared to SMA-confined NSC. These promising findings, especially for HSC, point to the possibility of the use of SMA spirals as a confinement technique to develop high-performance composite structural members in the construction industry.

5. Acknowledgements

The authors gratefully acknowledge the financial support from the National Natural Science Foundation of China through Grant No. 51650110495 and the University of Adelaide through a Research Excellence Grant awarded to the second author. The authors also thank Messrs. Giannini, Koch, Lim, and Shaw for completing the tests reported in this paper as part of their Honour's thesis.

6. References

[1] Idris Y and Ozbakkaloglu T 2013 *J. Compos. Constr*. **17(6)** 04013013.
[2] Ozbakkaloglu T and Lim J C 2013 *Compos. Part B*. **55** 607-634.
[3] Lim J C and Ozbakkaloglu T 2014 *J. Compos. Constr*. **18(4)** 04013058.
[4] Lim J C and Ozbakkaloglu T 2014 *Mag. Conc. Res*. **66(20)** 1020-1035.
[5] Ozbakkaloglu T and Idris Y 2014 *J. Struct. Eng.* **140(6)** 04014019.
[6] Dundar C, Erturkmen D and Tokgoz S 2015 *Eng. Struct.* **102** 31-39.
[7] Ozbakkaloglu T 2015 *Thin. Wall. Struct*. **96** 295-306.
[8] Xie T and Ozbakkaloglu T 2015 *Eng. Struct*. **90** 158-171.
[9] Mansouri I, Ozbakkaloglu T, Kisi O, and Xie T 2016 *Mater. Struct*. 10.1617/s11527-015-0790-4

[10] Xie T, Ozbakkaloglu T 2016 *Construct. Build. Mater*. **105** 132-143.
[11] Ozbakkaloglu T, Fanggi B A L, Zheng J 2016 *Mater. Des.* **96** 458-469.
[12] Chen L, Ozbakkaloglu T 2016 *Eng. Struct*. **117** 486-495.
[13] Ozbakkaloglu T, Saatcioglu M 2017 *Eng. Struct*. **147** 345-355.
[14] Lim J C and Ozbakkaloglu T 2014 *J. Compos. Constr*. 10.1061/ (ASCE) CC.1943-5614.0000536.
[15] Lim J C and Ozbakkaloglu T 2015 *J. Struct. Eng.* 10.1061/ (ASCE) ST.1943-541X.0001177.
[16] Lim J C and Ozbakkaloglu T 2015 *J. Struct. Eng.* **141(5)** 04014141.
[17] Lim J C and Ozbakkaloglu T 2016 *J. Mater. Civil Eng*. **28(2)** 06015010.
[18] Mansouri I, Gholampour A, Kisi O and Ozbakkaloglu T 2016 *Neural. Comput. Appl*. 10.1007/s00521-016-2492-4.
[19] Lim J C, Ozbakkaloglu T, Gholampour A, Bennett T and Sadeghi R 2016 *J. Struct. Eng*. 10.1061/ (ASCE) ST.1943-541X.0001589.
[20] Ozbakkaloglu T, Gholampour A and Lim J C 2016 *J. Compos. Construct.* 10.1061/ (ASCE) CC.1943-5614.0000712.
[21] Keshtegar B, Sadeghian P, Gholampour A, Ozbakkaloglu T 2017 *Compos. Struct*. **163** 423-431.
[22] Keshtegar B, Ozbakkaloglu T and Gholampour A 2017 *Eng. Comput.* **33(3)** 415-430.
[23] Moghaddam H, Samadi M, Pilakoutas K and Mohebbi S 2010 *Mater. Struct.* **43**, 1369-1381.
[24] Lim J C, Ozbakkaloglu T 2014 *Construct. Build. Mater*. **71** 492-509.
[25] Vincent T and Ozbakkaloglu T 2017 *J. Compos. Construct.* 10.1061/(ASCE)CC.1943-5614.0000802.
[26] Gholampour A, Ozbakkaloglu T and Hassanli R 2017 *Construct. Build. Mater*. **138** 372-382.
[27] Choi E, Nam T H, Cho S C, Chung Y S and Park T 2008 *Smart. Mater. Struct.* **17(6)** 065032.
[28] Choi E, Chung Y S, Choi J H, Kim H T and Lee H 2010 *Smart. Mater. Struct.* **19(3)** 035024.
[29] Shin M and Andrawes B 2010 *J. Eng. Struct*. **32(3)** 656-664.
[30] Park J, Choi E, Park K and Kim H T (2011) *Smart. Mater. Struct.* **20(9)** 094008.
[31] Dommer K and Andrawes B 2012 *J. Mater. Civ. Eng.* **24(10)** 1274-1282.
[32] Vincent T, Ozbakkaloglu T 2015 *J. Compos. Construct*. **19(6)** 04015003.
[33] Idris Y and Ozbakkaloglu T 2016 *Eng. Struct.* **118**, 307-319.
[34] Vincent T, Ozbakkaloglu T 2016 *Mater. Struct*. **49(4)** 1245-1268.
[35] Ozbakkaloglu T and Akin E 2012 *J. Compos. Construct.* **16(4)** 451-463.
[36] Ozbakkaloglu T 2013 *Eng. Struct*. **51** 188-199.
[37] Ozbakkaloglu T 2013 *J. Compos. Construct.* **17(1)** 151-161.
[38] Lim J C and Ozbakkaloglu T 2015 *Mater. Struct.* 48(9), 2839-2854.